The Temperature Dependence of Fundamental Photophysical Properties of $[Eu(MeOH\text{-}d_4)_9]^{3+}$ Solvates and $[Eu.DOTA(MeOH\text{-}d_4)]^-$ Complexes

Nicolaj Kofod, Lea Gundorff Nielsen, Thomas Just Sørensen

Nano-Science Center and Department of Chemistry, University of Copenhagen, Universitetsparken 5, 2100 København Ø, Denmark, tjs@chem.ku.dk

ABSTRACT: The trivalent lanthanide ions show optical transitions between energy levels within the 4*f* shell. All these transitions are formally forbidden according to the quantum mechanical selection rules used in molecular photophysics. Nevertheless, highly luminescent complexes can be achieved, and terbium(III) and europium(III) ions are particularly efficient emitters. This report started when an apparent lack of data in the literature led us to revisit the fundamental photophysics of europium(III). The photophysical properties of two complexes – $[Eu.DOTA(MeOH\text{-}d_4)]^-$ and $[Eu(MeOH\text{-}d_4)_9]^{3+}$ – were investigated in deuterated methanol at five different temperatures. Absorption spectra showed decreased absorption cross sections as the temperature was increased. Luminescence spectra and time-resolved emission decay profiles showed a decrease in intensity and lifetime as a temperature was increased. Having corrected the emission spectra for the actual number of absorbed photons and differences in the non-radiative pathways, the relative emission probability was revealed. These were found to increase with increasing temperature. The transition probability for luminescence was shown to increase with temperature, while the transition probability for light absorption decreased. The changes in transition probabilities were correlated to a change in the symmetry of the absorber or emitter, with an average increase in symmetry lowering absorption cross section and access to more asymmetric structures increasing the emission rate constant. Determining luminescence quantum yields and the Einstein coefficient for spontaneous emission allowed us to conclude that lowering symmetry increases both. Further, it was found that collisional self-quenching is an issue for lanthanide luminescence, when high concentrations are used. Finally, detailed analysis revealed results that show the so-called 'Werts' method' for calculating radiative lifetimes and intrinsic quantum yields are based on assumptions that do not hold for the two systems investigated here. We conclude that we are lacking a good theoretical description of the intraconfigurational *f-f* transitions, and that there are still aspects of fundamental lanthanide photophysics to be explored.

Introduction

Lanthanide luminescence is very intriguing from a standpoint of molecular photophysics. The experimentally observed optical transitions in both absorption and emission spectra are forbidden, and we rationalize the intense emission as lack of non-radiative deactivation processes. The hypothesis is that deactivation only occurs radiatively or via energy transfer, typically to overtones of vibrations in the solvent, which manifest as quenching. [1, 2]

While we are able to describe allowed electronic transitions from first principles, forbidden transitions are more tricky. Therefore, lanthanide luminescence is often rationalized using semi-empirical theories of varying quality e.g., some do not operate with conservation of energy. Most prominently featured in the literature are Latva's rule (empirical),[3] Judd-Ofelt theory (J-O theory, semi-empirical),[4] hypersensitivity (exception to J-O theory, empirical),[5] and Werts' method (derived from Judd-Ofelt theory)[6]. Of these, Latva's work and hypersensitivity rest securely on experimental evidence, while J-O theory describes most observations in solids.[7, 8] In our work—and starting to appear in the literature— we find data that is at odds with these theories. Therefore, we decided to consider the theories in detail by revisiting the fundamental photophysical properties of the lanthanide ions. We start with Eu^{3+}, as this is the best candidate for increasing our understanding.[9]

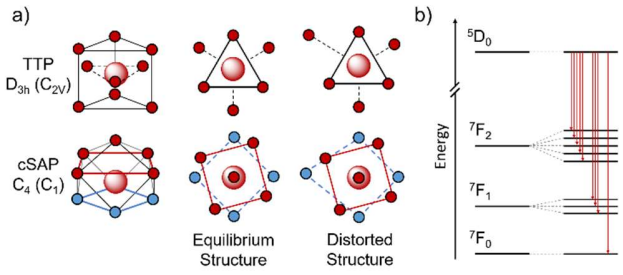

Figure 1. a) Solution structures of $[Eu(MeOH\text{-}d_4)_9]^{3+}$ (top) and $[Eu.DOTA(MeOH\text{-}d_4)]^-$ (bottom). The structures are a Tricapped Trigonal Prism (TTP) and a Capped Square Antiprism (cSAP) respectively. The indicated symmetries represent the point group symmetries of the equilibrium structures with the distorted structure symmetries in parenthesis. b) Energy levels in Eu^{3+}. The Russel-Saunders terms (left) are split by the ligand field to form microstates (right). The number of non-degenerate microstates depends on the ligand field symmetry.[10, 11] The main emissive state ($^5D_0$) and lowest lying electronic state ($^7F_0$) are both non-degenerate.

Eu^{3+} is the most studied member of the lanthanide series with regards to photophysical properties.[6, 9-12] This is due to a number of factors reducing the experimental complexity when investigating electronic energy levels and the transitions between them: *i*)The main transitions in both absorption and emission lie in the visible range allowing the use of widely available instrumentation. *ii*) The lowest lying electronic state ($^7F_0$) and main emissive state ($^5D_0$) are both non-degenerate, significantly simplifying the optical spectra, see Figure 1. *iii*) The excited state lifetime is in the ms range allowing for simple experimental detection. And, *iv*) Compared to other lanthanides the intrinsic quantum yield is high. Further motivation for the many studies come from a technical standpoint, where the characteristic red luminescence has been used in LED's, anti-counterfeiting as well as bio-assays and bio-imaging.[13-15] Despite the large body of work, our detailed studies indicate that the theoretical foundation for understanding Eu^{3+} luminescence is lacking. Thus, we set out to probe the fundamental photophysical properties of Eu^{3+} in two model systems: $[Eu(MeOH\text{-}d_4)_9](CF_3SO_3)_3$ and $[Eu.DOTA(MeOH\text{-}d_4)]^-$ in methanol-d_4. The structures of the complexes are shown in Figure 1 along with the electronic energy levels of Eu^{3+}. Methanol-d_4 was chosen to remove as many of the proton mediated non-radiative pathways as possible, and to reduce or remove complications from pH, while retaining a well-defined tricapped trigonal prismatic (TTP) and capped square anti-prismatic (cSAP) coordination geometry, see Figure 1. The $CF_3SO_3^-$ salt of Eu^{3+} was chosen as it is known to form only outer sphere complexes in methanol.[16] Similarly, DOTA (1,4,7,10-Tetraazacyclododecane-1,4,7,10-tetraacetic acid) was chosen as the structure of DOTA complexes of the trivalent lanthanide ions have been studied in great detail.[17, 18]

In earlier work we have determined the solution structure of $[Eu(MeOH\text{-}d_4)_9]^{3+}$ to be a tricapped trigonal prism.[16] The structure of $[Eu.DOTA(MeOH\text{-}d_4)]^-$ is well known to be a capped square antiprism.[19] These two structures are the most common structures for 9-coordinated complexes of trivalent lanthanides, as they based on electrostatics resemble the two lowest energy conformations.[20, 21]

Ln^{3+} complexes in solution are dynamic systems.[18] The ligand exchange for trivalent lanthanides is fast – it ocurs on the ns timescale.[18, 19, 22, 23] As such structural fluctuations play a significant role in the observed properties of lanthanide complexes in solution[22, 24] and as we study dynamic systems it is important to consider the time-scale of the exchange processes of the system as well as the time-scale of the experiment.[24] Absorption and emission spectroscopy both probe electronic transitions but there is a large difference in the experimental time-scale. Absorption (fs) can always be considered instantaneous compared to molecular motion (ns or slower), and thus gives a snapshot of the species in solution. In emission experiments, the excited state lifetime is the determining factor. For Eu^{3+} this can be as long as several ms, which compared to the ligand exchange and molecular motion (ns) is a slow process, and these may induce significant effect on the observed properties, see Figure 2.[22, 24]

Here, we study $[Eu(MeOH\text{-}d_4)_9]^{3+}$ and $[Eu.DOTA(MeOH\text{-}d_4)]^-$ at temperatures from 10°C to 50 °C. We expect that the highest symmetry form of the complexes has the lowest energy. While an increase in temperature will cause conformational fluctuations to occur more readily, it will also allow forms with an overall decrease in the point group symmetry to become accessible. Whether the average symmetry of the ligand field increase or decrease as low-symmetry, high energy conformations becomes transiently populated is impossible to know, but we can consider the general effect of temperature on the population of the different forms of the complexes, see Figure 2.

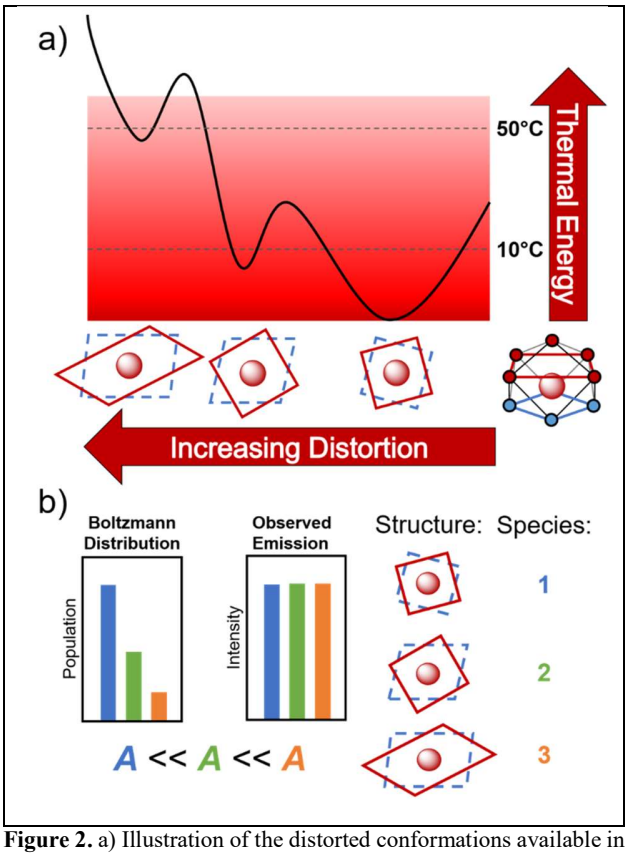

Figure 2. a) Illustration of the distorted conformations available in $[Eu.DOTA(MeOH\text{-}d_4)]^-$. At lower temperatures, the exchange between these is slow. Thus, a species can be temporarily 'trapped' in a low symmetry conformation. At higher temperatures, the exchange becomes fast and the species will move out of the less favorable, less symmetric conformation faster. It also allows new, less symmetrical conformations to be populated. The effect is that the average ensemble of structures will be more symmetric at higher temperatures, but less symmetrical structures will also be populated. As symmetry is directly related to transition probability, this dictates the spectral changes observed in the experiments (see main text). b) Illustration of the effect of weighted averages on the observed emission. Considering three different conformations of a complex: **1** (blue), **2** (green) and **3** (orange). **1** is more symmetric than **2**, which is more symmetric than **3**. The transition probability (***A***) is in the reverse order, as dictated by the ligand field symmetry. Because the excited state lifetime is several orders of magnitude slower (ms range) compared to molecular motion (ns) range a complex may visit all three conformations before emission occurs. If the probability of emission is significantly higher for one conformation, compared to the other, this will result in an overrepresentation of the emission signal from that species. In the example shown here, **1** has a population of twice that of **2** and five times that of **3**. However, the emission probability of **1** is half that of **2** and a fifth of that of **3**. The resulting emission spectra will therefore give an overrepresentation of the asymmetric species.

In molecular photophysics the theoretical description of 'forbidden' electronic transitions remains poor, and similarly our ability to treat the lanthanide centered excited states is limited.[25] We classify the transitions using black body radiation, the Strickler-Berg equations, and Einstein's theory of stimulated absorption and spontaneous emission.[26, 27] For a given electronic transition the rate constants of—or Einstein's coefficient for—spontaneous emission ***A*** is conveniently linked to the quantum mechanical transition dipole operator, which we in more loosely defined terms can link to the experimentally determined oscillator strength *f*.[28, 29] The oscillator strength is a convenient measure as it provides a physical constant that can be used on any band, disregarding the number of lines present.[30] For Eu^{3+} we can go a step further and use $\boldsymbol{A}_{\mathbf{rel}}$ as the emissive state is non-degenerate, see Figure 1. This allows us to experimentally determine transition probabilities and challenge the current theoretical models. In J-O theory we already know that some bands are poorly described, and it was recognized early that it was necessary to separate bands in 'pure' and 'hypersensitive' depending on whether they could be described by the theory or not.[5] Further, some of the inherent assumption require mixing of isoenergetic excited electronic energy levels, which is incompatible with experimental data.[31] Finally, J-O theory predicts the nature of the transitions as electric dipole, magnetic dipole, and induced electric dipole. We do not consider these assignments to have merit, and assume that all interactions between light and matter are dominated by an electric field operator.[11] This has significant consequences for the Werts' method as shown below. These consequences should be noted as it is a widely used tool in analysis of Eu^{3+} luminescence.

This work started as we noticed significant changes in the spectra of $[Eu(MeOH\text{-}d_4)_9]^{3+}$ and $[Eu.DOTA(MeOH\text{-}d_4)]^-$ in methanol-d_4 as a function of temperature. To investigate further, we determined the photophysical properties of Eu^{3+} in these two complexes at 10, 20, 30, 40 and 50°C. This was done as a combination of absorption, steady state, and time-resolved emission spectroscopies. The data was used to determine the changes in absorption cross section, excited state lifetime, luminescence quantum yield, and the rate constants for spontaneous emission and non-radiative deactivation (k_r and k_{nr}). From the data we can conclude that the absorption transition probability decreases and the emission transition probability increases with increasing temperature in both systems. This we can explain by the differences in the experimental time-scale. We can also conclude that k_r increases with increasing temperature, while k_{nr} remains constant. Further, by determining k_r we can evaluate the Werts' method for determining this constant in Eu^{3+} complexes, and we find the method does not work for the systems studied here.

Methods and Materials

Sample Preparation. $Eu(CF_3SO_3)_3$ (98% Strem Chemicals) was used as received. $H_3O[Eu(DOTA)]$ was prepared by literature procedure[32, 33] and purified using Ion-Exchange Chromatography (see SI). Both samples were dissolved in MeOH-d_4 (Eurisotop). Samples were kept in 10 mm quartz cuvettes from Starna Scientific with a screw top. The cuvettes were further sealed with Parafilm M (Sigma-Aldrich). This was done to prevent contamination from water. To check the sample integrity, the excited state lifetime was evaluated over time, the observed change was consistent yet of a magnitude that was deemed insignificantly compared to all other changes observed in these experiments.

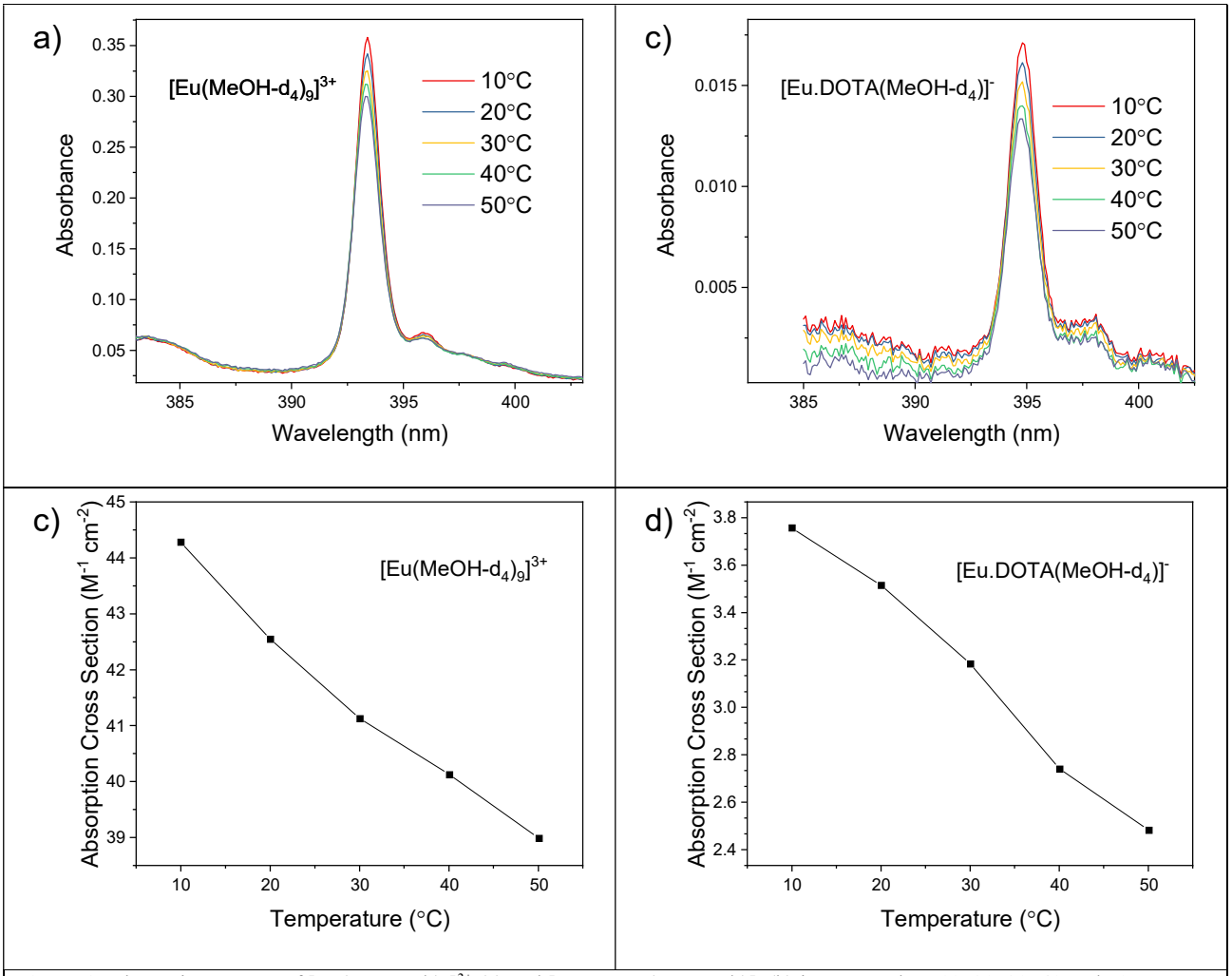

Figure 3. Absorption spectra of $[Eu(MeOH\text{-}d_4)_9]^{3+}$ (a) and $[Eu.DOTA(MeOH\text{-}d_4)]^-$ (b) in MeOH-d_4 at 10, 20, 30, 40 and 50 °C. Area of the absorption cross section in the excitation window (394 nm ± 8 nm) of $[Eu(MeOH\text{-}d4)_9]^{3+}$ (c) and $[Eu.DOTA(MeOH\text{-}d_4)]^-$ (d) as a function of temperature. Lines are a guide for the eyes only.

Optical Spectroscopy. Absorption spectra were recorded using a Cary-300 double-beam spectrometer from Agilent Technologies using air as a reference with zero/baseline correction on the cuvette containing only solvent. Slits were kept at 1 nm. Temperature control was achieved with a water pump and a Cary Single Cell Peltier Accessory. A minimum of 30 minutes of equilibration time allowed the system to stabilize at each temperature. A constant nitrogen flow was sent through the sample chamber to avoid condensation on the cuvettes. For $[Eu.DOTA(MeOH\text{-}d_4)]^-$ the average of 5 runs were used to reduce noise.

Emission spectra were carried out on a PTI QuantaMaster 8075 instrument from Horiba Scientific using a Xenon lamp for excitation. Excitation wavelength was 394 nm. Excitation and emission slits were 8 nm and 1.5 nm respectively. The emission intensity was corrected for wavelength-dependent detector sensitivity using a factory provided correction file. Fluctuations in lamp intensity was corrected using a reference detector with a factory provided correction file. Time-resolved emission decay profiles were recorded on the same instrument using a Xenon flash lamp as the excitation source. Excitation and emission were done at 394 nm and 700 nm with 8 nm excitation slits and 8 nm emission slits. The time-gate was set at 300 μs to remove all residual signal from the lamp. The decay profiles were fitted using a single-exponential decay function in the Origin 2020 (OriginLab) software package. In the steady-state and time-resolved measurements, the temperatures were controlled using a Koolance EXT-440 liquid cooling system from Horiba Scientific. A minimum of 30 minutes of equilibration time allowed the system to stabilize at each temperature. A constant nitrogen flow was sent through the sample chamber to avoid condensation on the cuvettes.

No signals from other Ln^{3+} ions were detected in any measurements.

Quantum Yield Determination. For Quantum Yield measurements, we attempted the IUPAC recommended, relative, five-point dilution method.[34-36] However, due to self-quenching effects (see below), only single point determinations were possible. Coumarin-153 in ethanol was used as a reference. Absorption spectra were recorded on the Cary-300 setup (see above). For the $[Eu.DOTA(MeOH\text{-}d_4)]^-$ spectra, a five run average was used to reduce noise. Slits were kept at 4 nm. The temperature was kept constant at 20 °C. A minimum of 30 minutes of equilibration time allowed the

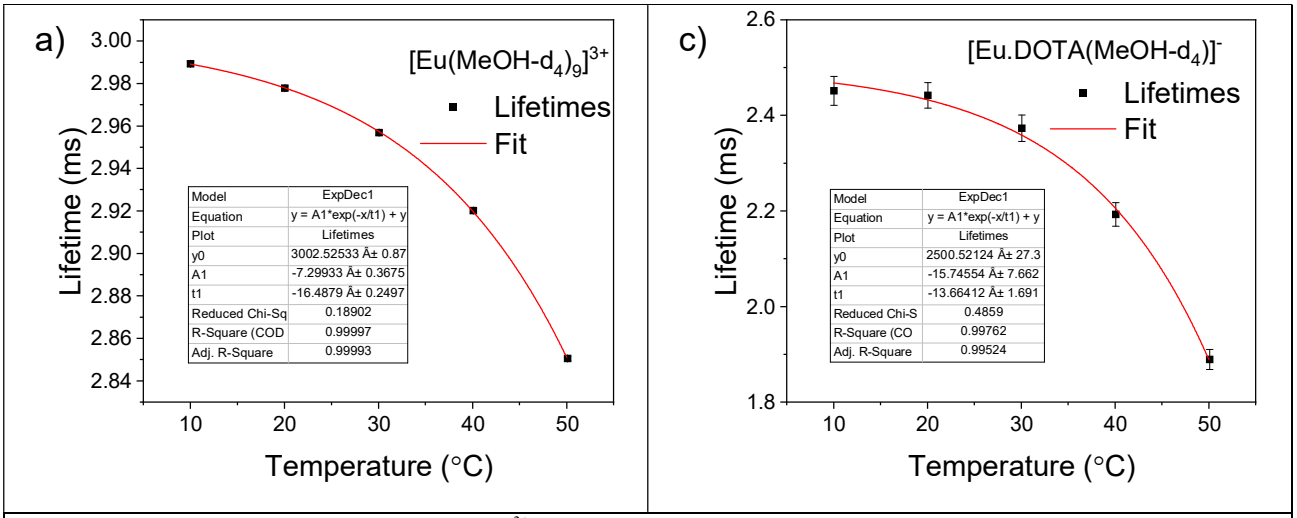

Figure 4. Excited state lifetime of $[Eu(MeOH\text{-}d4)_9]^{3+}$ (a) and $[Eu.DOTA(MeOH\text{-}d_4)]^-$ (b) in MeOH-d_4 as a function of temperature. The data has been fitted with a mono-exponential decay function.

system to stabilize at this temperature. Emission spectra were recorded on the PTI QuantaMaster 8075 (see above). Excitation was done at 394 nm. Excitation and emission slits were kept constant at 4 nm and 1.5 nm respectively. Absorption was kept below 0.12 for all samples to reduce inner-filter effects. This is slightly above the IUPAC recommended 0.1 limit, but did not affect linearity in the measurements.

Self-quenching experiments. To further probe the self-quenching effects observed in the Quantum Yield determinations (see below) a dilution experiment of $Eu(CF_3SO_3)_3$ in MeOH (HPLC-grade, from Sigma-Aldrich) was performed. The absorption and emission spectra were recorded on one set of samples, while the lifetime-measurements were performed on a second set. This was done to avoid changing slits and mirrors between steady-state and time-resolved settings in the instrument. The absorption and emission spectra were carried out on the instruments described above. Absorption slits were kept at 4 nm. Excitation and emission slits were kept at 4 nm and 1.5 nm respectively. For lifetime measurements excitation was done at 394 nm and emission was measured at 700 nm with slits set at 4 nm and 8 nm for excitation and emission respectively. No temperature control was used for the absorption measurements. For the emission and lifetime measurements temperature was kept constant at 20 °C. An additional five-point dilution was performed on Coumarin-153 to probe detector linearity.

Determining Relative Transition Probabilities. In this study, the focus is on the transition specific radiative rate constant k_r and the effect of temperatures on this. k_r correlates directly to Einstein's spontaneous emission coefficient, $\boldsymbol{A}$. Obtaining $\boldsymbol{A}$ is a tedious process and requires at least a good experimental determination of luminescence lifetimes, quantum yields, and the energy and intensity of the '0-0' transition. This is often exceedingly difficult for Ln^{3+} ions. In order to circumvent these issues we compare the relative changes across a set of samples with identical concentrations of the emitter.[16, 24] This allows for a number of simplifications to be applied. We can obtain the relative Quantum Yield from equation 1

$$\Phi_{rel} = \frac{\int I^E(\lambda)d\lambda}{Abs}, \Phi^{\lambda}_{rel} = \frac{I^E}{Abs} \qquad \textbf{eq. 1}$$

Where Φ_{rel} is the relative quantum yield, I^E is the emission intensity and Abs fraction of absorbed photons in the excitation window. This corrects the emission spectra for changes in the number of absorbed photons. The quantum yield relates directly to the radiative rate constant k_r by equation 2.

$$\Phi = \frac{k_r}{k_r + k_{nr}} = \frac{k_r}{k_{obs}} \qquad \textbf{eq. 2}$$

Where k_r is the radiative rate constant, k_{nr} is the rate constant for non-radiative deactivation, and k_{obs} is the sum of all radiative and non-radiative rate constants leading away from the excited state. As k_r and $\boldsymbol{A}$ are directly related, the relative quantum yield can thus be used to determine the relative transition probability $\boldsymbol{A}_{rel}$ by equation 3

$$\Phi_{rel} = \frac{\boldsymbol{A_{rel}}}{k_{obs}}, \boldsymbol{A_{rel}} = \Phi_{rel} \cdot k_{obs}, \boldsymbol{A_{rel}} = \frac{\Phi_{rel}}{\tau_{obs}} \qquad \textbf{eq. 3}$$

Where $\boldsymbol{A}_{rel}$ is the relative transition probability and τ_{obs} is the observed excited state lifetime. This corrects for the changes in non-radiative pathways affecting the emission intensity. It should be noted that the $\boldsymbol{A}_{rel}$ obtained is directly proportional - but not equal -to the Einstein Coefficient of spontaneous emission $\boldsymbol{A}$. This treatment ensures that the changes observed in the emission spectra are only due to changes in the intrinsic emission transition probability and are not affected by changes in the number of absorbed photons or changes in the non-radiative pathways. Additionally, this method is only applicable to Eu^{3+} since the ground state and main emissive states are non-degenerate. In systems with degenerate absorbing or emitting states this treatment cannot be used, in particular where changes in degeneracy occur

Results and Discussion

Effect of Temperature on Light Absorption.

Figure 3 shows the absorption spectra of $[Eu(MeOH\text{-}d_4)_9]^{3+}$ and $[Eu.DOTA(MeOH\text{-}d_4)]^-$ at 10 °C, 20 °C, 30 °C, 40 °C and 50 °C. As the temperature increases there is no significant broadening of the absorption band, see Tables 1 and 2. This is in contrast to what is seen for organic fluorophores as well as transition metal emitters, where the vibronic coupling is more pronounced.[37]

As the temperature increases, the absorption cross-section decreases. This is unexpected. Increasing temperatures must lead to increasing structural fluctuations. In the assumption that the intra-configurational transition of Ln^{3+} ions occur due to a breakdown of symmetry, asymmetric structures have higher intrinsic transition probabilities than symmetric structures.[9, 11, 16,

[24, 29, 38, 39] Thus, it would be expected that increased structural fluctuations would lead to a lowering of the symmetry, in turn leading to an increase in transition probability. What we observe here is the opposite. This can be explained by considering the different structures in solution and the population of these. The increased thermal fluctuations ensure that no complex is trapped in asymmetric local minima, and thus lead to a total population of complexes that at any given point in time adopt a more symmetrical structure ensemble. This leads to an overall decrease in transition probability as temperatures increase. The concept is illustrated in Figure 2.

Table 1. Linewidths of optical transition bands in [Eu.DOTA(MeOH-d4)]- in MeOH-d4 at 10-50°C

[Eu.DOTA(MeOH-d4)]-					
Absorption FWHM (cm^{-1})[a]					
	10°C	20°C	30°C	40°C	50°C
394 nm Band	96	103	103	103	103
Emission FWHM (cm^{-1})[a]					
	10°C	20°C	30°C	40°C	50°C
$^5D_0 \rightarrow {}^7F_0$ (Full)	50	50	53	50	50
$^5D_0 \rightarrow {}^7F_1$ (Full)	297	303	306	308	314
$^5D_0 \rightarrow {}^7F_2$ (Peak)	118	121	123	123	123
$^5D_0 \rightarrow {}^7F_2$ (Full)	431	431	431	428	428
$^5D_0 \rightarrow {}^7F_3$ (Peak)	60	63	65	65	67
$^5D_0 \rightarrow {}^7F_3$ (Full)	214	216	219	219	223
$^5D_0 \rightarrow {}^7F_4$ (Peak1)	52	57	57	57	57
$^5D_0 \rightarrow {}^7F_4$ (Peak2)	57	59	61	61	59
$^5D_0 \rightarrow {}^7F_4$ (Full)	493	491	491	491	493

[a] We estimate an uncertainty of ±13 cm^{-1} for absorption and ±6 cm^{-1} for emission experiments based on the step size (0.1 nm)

Table 2. Linewidths of optical transition bands in $[Eu(MeOH\text{-}d_4)_9]^{3+}$ in MeOH-d4 at 10-50 °C

$[Eu(MeOH\text{-}d_4)_9]^{3+}$					
Absorption FWHM (cm^{-1})[a]					
	10°C	20°C	30°C	40°C	50°C
394 nm Band	90	90	90	97	97
Emission FWHM (cm^{-1})[a]					
	10°C	20°C	30°C	40°C	50°C
$^5D_0 \rightarrow {}^7F_1$ (Full)	247	250	252	252	255
$^5D_0 \rightarrow {}^7F_2$ (Full)	317	322	322	319	322
$^5D_0 \rightarrow {}^7F_3$ (Peak)	82	85	87	92	92
$^5D_0 \rightarrow {}^7F_3$ (Full)	330	330	332	332	332
$^5D_0 \rightarrow {}^7F_4$ (Peak)	81	83	81	83	87
$^5D_0 \rightarrow {}^7F_4$ (Full)	324	326	330	334	336

[a] We estimate an uncertainty of ±13 cm^{-1} for absorption and ±6 cm^{-1} for emission experiments based on the step size (0.1 nm)

Effect of Temperature on Luminescence.

Figure 4 shows the excited state lifetimes of $[Eu(MeOH\text{-}d_4)_9]^{3+}$ and $[Eu.DOTA(MeOH\text{-}d_4)]^-$ as a function of temperature. The time-resolved emission decay profiles from which the lifetimes were obtained can be found in Figure S3 and S15. As the temperature increases the excited state lifetime decreases. The observed lifetime is defined in equation 4.

$$\tau_{obs} = \frac{1}{k_r + k_{nr}} \qquad \textbf{eq. 4}$$

Thus, the decrease can be the result of an increase in k_r and/or k_{nr}.[40] The fact that the overall intensity of the emission spectra decreases with increasing temperature (Figures S5-6 and S17-18) would indicate that it is due to an increase in k_{nr}. However, this is where it is important to note that the absorption also decreases as temperatures increases, so the decrease in intensity could also be due to this. For both $[Eu(MeOH\text{-}d_4)_9]^{3+}$ and $[Eu.DOTA(MeOH\text{-}d_4)]^-$ the decrease in absorption is significantly larger than the observed decrease in emission intensity. As in the absorption spectrum, there is no significant broadening of the emission spectrum observed at the temperature increase, see Tables 1 and 2.

Figure 5 shows the relative transition probability A_{rel} (see experimental section) of emission of $[Eu(MeOH\text{-}d_4)_9]^{3+}$ and $[Eu.DOTA(MeOH\text{-}d_4)]^-$. In contrast to the emission intensity, A_{rel} increases overall as the temperature is increased. This indicates a decrease in the symmetry of the complex. Initially this seems to contradict the observations from the absorption spectra, where the transition probability decreased with increasing temperatures. However, this can be explained by looking at the experimental timescale of the two processes.[16, 24] Compared to molecular motion and ligand exchange in Ln^{3+} complexes, which are both in the ns range, absorption (fs) can be considered instantaneous. Therefore, the absorption spectra give a snapshot of the average structure. Emission is in the ms range. This allows for a number of conformations to be visited during the excited state lifetime. As probability of emission correlates directly to the symmetry of the ligand field some of these conformations will have significantly faster rates of spontaneous emission, see illustration in Figure 2. The increase in temperature will increase the structure fluctuations and also the number of times an electronically excited Eu^{3+} can visit a distorted structure. Thus, A_{rel} increases as temperature increases.

Revisiting Europium(III) photophysics.

By fully appropriating the prevalent theoretical treatment of the intraconfigurational *f-f* transition, Werts—among others—proposed that the $^5D_0 \rightarrow {}^7F_1$ transition has purely magnetic dipole character.[6, 8, 41, 42] As magnetic dipole transitions following first principle arguments are symmetry allowed (yet nominally forbidden due to spin-conservation, momentum conservation, and parity),[28, 30, 43] they are not affected by the ligand field symmetry. While there is no empirical evidence nor traditional photophysical rationale as to why the $^5D_0 \rightarrow {}^7F_1$ transition should be purely magnetic in nature, Werts' argument has led to a methodology where the $^5D_0 \rightarrow {}^7F_1$ transition is used as an internal anchor for determining photophysical properties of Eu^{3+} complexes. Werts has proposed equation 5 as a method for determining the radiative rate constant for Eu^{3+} complexes.

$$k_r = A_{MD} \cdot n^3 \cdot I_{tot}/I_{MD} \qquad \textbf{eq. 5}$$

Where A_{MD} is the Einstein Coefficient of spontaneous emission for the $^5D_0 \rightarrow {}^7F_1$ transition in vacuo, calculated to be 14.65 s^{-1}, n is the refractive index of the solvent, I_{tot} is the total integrated emission intensity (often ignoring the weak bands at 750 and 825 nm), and I_{MD} is the intensity of the $^5D_0 \rightarrow {}^7F_1$ transition band. Our data has never been consistent with this methodology,[16, 24] and we decided to document this fact here.

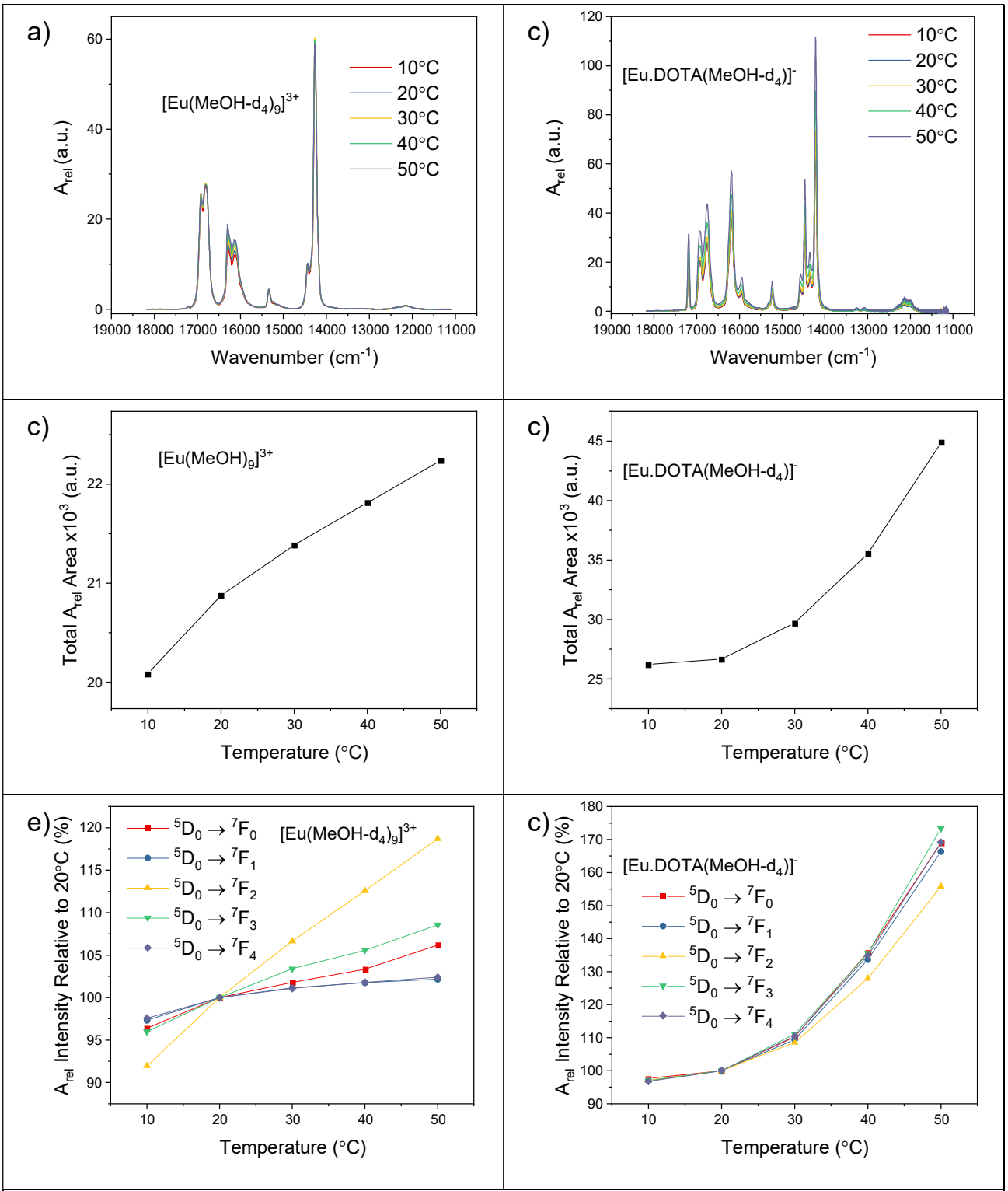

Figure 5. Relative emission probability, A_{rel} (see experimental section) of $[Eu(MeOH\text{-}d_4)_9]^{3+}$ (a) and $[Eu.DOTA(MeOH\text{-}d_4)]^-$ (b) in MeOH-d_4 at 10, 20, 30, 40 and 50°C. Integrated relative emission probability (A_{rel}) as a function of temperature for $[Eu(MeOH\text{-}d_4)_9]^{3+}$ (c) and $[Eu.DOTA(MeOH\text{-}d_4)]^-$ (d) in MeOH-d_4. Lines are a guide for the eyes only. A_{rel} intensity (see experimental section) of the individual emission bands relative to the intensity at 20 °C of $[Eu(MeOH\text{-}d_4)_9]^{3+}$ (e) and $[Eu.DOTA(MeOH\text{-}d_4)]^-$ (f) in MeOH-d_4 as a function of temperature. Lines are a guide to the eyes only.

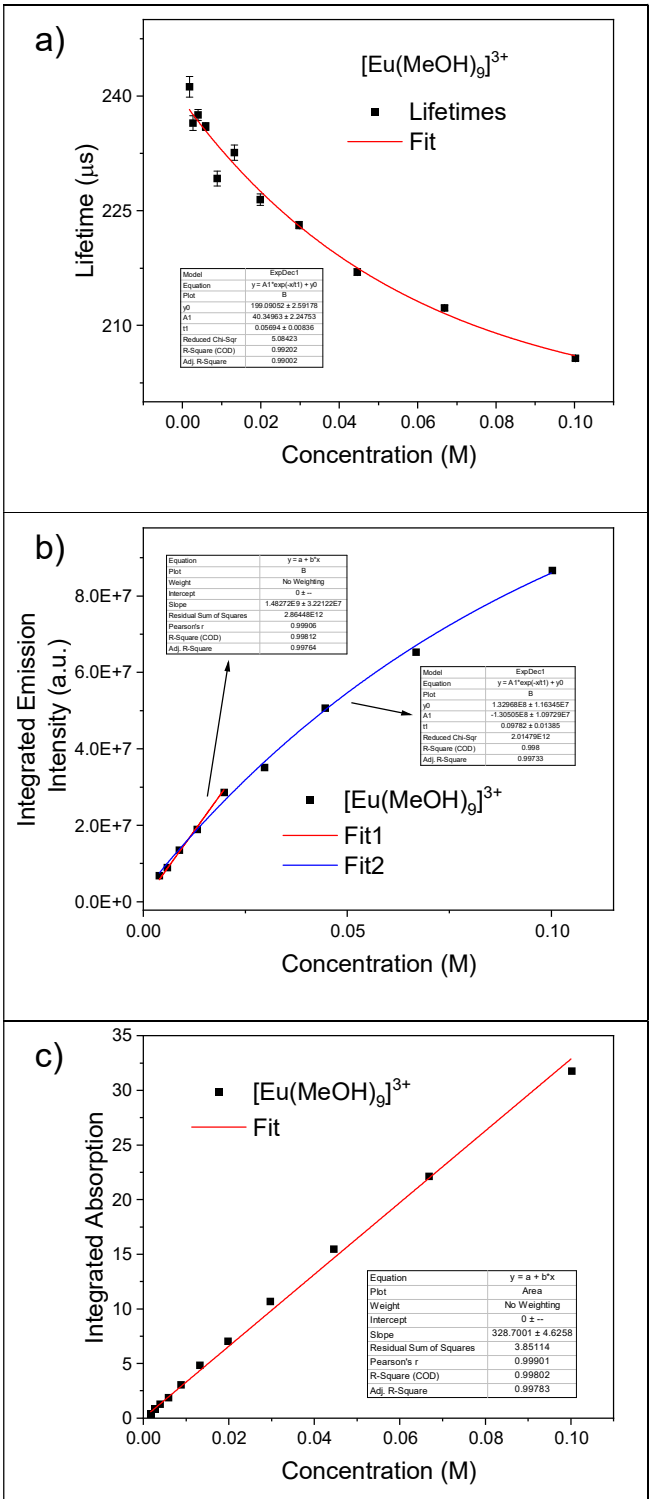

Figure 6. a) Excited state lifetime of $[Eu(MeOH)_9]^{3+}$ in MeOH as a function of temperature. The data has been fitted with mono-exponential decay function. b) Integrated emission intensity of $[Eu(MeOH)_9]^{3+}$ in MeOH as a function of temperature. The full data set has been fitted with a mono-exponential decay function (blue). The 4 lowest concentration points has been fitted with a linear function (red). c) Integrated absorption cross section of $[Eu(MeOH)_9]^{3+}$ in MeOH in the excitation window (394 nm ± 4 nm). The data has been fitted with a linear function.

Figure 5 shows A_{rel} of the individual emission bands of $[Eu(MeOH\text{-}d_4)_9]^{3+}$ and $[Eu.DOTA(MeOH\text{-}d_4)]^-$ relative to the 20 °C sample. Please note that we are using bands and not transitions (lines) to describe the spectral features. Each band contains several transitions between the individual m*J* levels, microstates or j-states within each Russel-Saunders term. It is only when both Russel-Saunders denoted spin-orbit levels are non-degenerate that we observe a line *i.e.* a spectral feature that arise from a single electronic transition.

For $[Eu(MeOH\text{-}d_4)_9]^{3+}$ the $^5D_0 \rightarrow {}^7F_1$ band has the lowest variance. However, it is not constant. It also has a similar relative change to the $^5D_0 \rightarrow {}^7F_4$ band, which is J-O theory describes as both purely electric dipole in nature and hypersensitive (that is the intensity cannot be described by Judd-Ofelt theory).[5, 8] As such, the same theory Werts exploits dictates that the $^5D_0 \rightarrow {}^7F_4$ band should highly sensitive to changes in ligand field symmetry and the relative change in A_{rel} for the $^5D_0 \rightarrow {}^7F_4$ band should thus be expected to be significantly higher than that for the $^5D_0 \rightarrow {}^7F_1$ band.

For $[Eu.DOTA(MeOH\text{-}d_4)]^-$ the $^5D_0 \rightarrow {}^7F_1$ band has a higher relative change than the $^5D_0 \rightarrow {}^7F_2$ band which is also described as hypersensitive.[5, 10, 44] Hypersensitive transition are supposedly exceedingly sensitive to changes in the ligand field symmetry and should thus experience the largest relative change, as is the case in $[Eu(MeOH\text{-}d_4)_9]^{3+}$. These observations show that the $^5D_0 \rightarrow {}^7F_1$ band is not independent on the chemical environment of the Eu^{3+} ion. To examine this further we set out to determine the true radiative transition probability – that is Einstein probabilities for spontaneous emission *A* – by determining the luminescence quantum yield of $[Eu(MeOH\text{-}d_4)_9]^{3+}$ and $[Eu.DOTA(MeOH\text{-}d_4)]^-$.

Self-quenching of Europium(III). The IUPAC recommended 5-point dilution method for relative determination of quantum yields was attempted. [34-36] As can be seen in Figure S31 and S36 the absorption of the complexes is linear as a function of concentration. However, the integrated emission intensity is not linear, see figure S33 and S38. Instead it can accurately be described using a mono-exponential decay. As can be seen in Figure S38, the integrated emission intensity for $[Eu.DOTA(MeOH\text{-}d_4)]^-$ becomes linear at low concentrations. This indicates that the effect comes from self-quenching. To confirm this a dilution experiment using $Eu(CF_3SO_3)_3$ in protonated methanol was performed. The results can be seen in Figure 6. The absorption (Figure 6C) is linear throughout the dilution series. The excited state lifetime (Figure 6A) decreases at higher concentrations, while the emission intensity (Figure 6B) is non-linear. The last four points in the emission series (<0.02M) shows some linearity. The self-quenching effect is less pronounced in MeOH than in MeOH-d_4 due to the longer excited state lifetime in MeOH-d_4 as this allows more time for collisional self-quenching. Because of this effect our quantum yield determination is based on single point approach. Considering our data, we estimate that the quantum yield of Eu^{3+} will be independent of concentration at concentrations below 10 mM in protonated solvents and below 4 mM in deuterated solvents.

The photophysical properties are compiled in Table 3, all data is provided as Supporting Information. Cursory inspection of Table S2 shows that the quantum yield of $[Eu(MeOH\text{-}d_4)_9]^{3+}$ at 0.1 M concentration is lower than that for $[Eu.DOTA(MeOH\text{-}d_4)]^-$ at 5 mM. At lower concentrations, < 30mM, the quantum yield of $[Eu(MeOH\text{-}d_4)_9]^{3+}$ becomes comparable to that of $[Eu.DOTA(MeOH\text{-}d_4)]^-$. We expect that k_r remains constant

throughout dilution and that the increase in quantum yield is due to a decrease in k_{nr}. This is supported by the dilution measurements in MeOH, see Table S1. Here the k_{nr} decreases as the concentration decreases while the k_r remains constant within the experimental uncertainty.

Having considered the possible artifacts, we are ready to analyze the photophysical parameters compiled in Table 3. We note that k_r for $[Eu(MeOH\text{-}d_4)_9]^{3+}$ is lower than that for $[Eu.DOTA(MeOH\text{-}d_4)]^-$. This is consistent with the expected point group symmetries of the two complexes as the TTP structure and 9O donor set of $[Eu(MeOH\text{-}d_4)_9]^{3+}$ is the more symmetric than the cSAP structure and 4O, 4N, $1O^{\ddagger}$ donor set of DOTA. From the determined k_r we can use equation 5 to calculate the A_{MD} value of the $^5D_0 \rightarrow {}^7F_1$ transition. Our experimentally determined A_{MD} values are $20.46 s^{-1}$ and $18.45 s^{-1}$ for $[Eu.DOTA(MeOH\text{-}d_4)]^-$ and $[Eu(MeOH\text{-}d_4)_9]^{3+}$ respectively. Thus we provide experimental proof that the $^5D_0 \rightarrow {}^7F_1$ band is not insensitive to the environment as the experimentally determined values both change as a function of temperature (Table 4), and are significantly different from the $14.65\ s^{-1}$ proposed by Werts (Table 3).

Table 3. Photophysical data of $[Eu.DOTA(MeOH\text{-}d_4)]^-$ and $[Eu(MeOH\text{-}d_4)_9]^{3+}$ in MeOH-d_4 at 20 °C.

	$[Eu.DOTA(MeOH\text{-}d_4)]^-$	$[Eu(MeOH\text{-}d4)_9]^{3+}$
τ_{obs} (ms)	2.442(0.026)	2.977(0.001)
Φ^a	0.47 ±0.05	0.37±0.04
k_r (s^{-1})	$1.92 \cdot 10^2$ ±20	$1.26 \cdot 10^2$ ±13
k_{nr} (s^{-1})	$2.18 \cdot 10^2$ ±22	$2.10 \cdot 10^2$ ±21
A_{MD} (s^{-1})	20.46 ±2	18.45 ±2

[a] We estimate a relative uncertainty on the determined quantum yield based on the statistical error of absorption and emission data of the lowest concentration sample (see SI) added to the error on the reference quantum yield[34].

Effect of Temperature on Europium(III) Photophysics.

Using the luminescence quantum yield of $[Eu(MeOH\text{-}d_4)_9]^{3+}$ and $[Eu.DOTA(MeOH\text{-}d_4)]^-$ determined at 20 °C, we can determine the relative luminescence quantum yields for the entire temperature series. The results are summarized in Table 4.

The quantum yield of $[Eu.DOTA(MeOH\text{-}d_4)]^-$ increases significantly from 10 °C (46 %) to 50 °C (61 %). This is reflected in a large increase in k_r, while k_{nr} remains constant within error, see Table 4. The lack of temperature dependence on k_{nr} seems counterintuitive at first. However, it can be explained by the FRET-mechanism of non-radiative deactivation, which is the main pathways of k_{nr} in lanthanides[1, 2, 45, 46] The FRET-mechanism has no temperature dependent component and thus the k_{nr} is largely unaffected by the temperature increase.

The data in Table 4 show that the increase in k_r is significantly lower for $[Eu(MeOH\text{-}d_4)_9]^{3+}$ than it is for $[Eu.DOTA(MeOH\text{-}d_4)]^-$. This can be explained by the lack of symmetry breaking motions of the ligand sphere in the $[Eu(MeOH\text{-}d_4)_9]^{3+}$ complex, see Figure 1. Any vibrational modes in the ligand will in $[Eu(DOTA)MeOH\text{-}d_4]^-$ decrease the point group symmetry from a C_4 symmetry to a C_1. In $[Eu(MeOH\text{-}d_4)_9]^{3+}$ any single distortion of the coordinating ligands will leave one or more of the rotation axes intact. The $[Eu.DOTA(MeOH\text{-}d_4)]^-$ thus goes from a tetragonal class symmetry to a triclinic class symmetry, while the $[Eu(MeOH\text{-}d_4)_9]^{3+}$ goes from a hexagonal class symmetry to a rhombic class symmetry.[11]

k_{nr} for $[Eu(MeOH\text{-}d_4)_9]^{3+}$ is constant within our experimental uncertainty in the temperature range. This is somewhat surprising when considering the self-quenching we observed in the dilution experiments mentioned above. However, in terms of the number of collisions per second in solution a temperature increase of 40 °C is insignificant.[47]

Table 4. Photophysical data of $[Eu.DOTA(MeOH\text{-}d_4)]^-$ and $[Eu(MeOH\ d_4)_9]^{3+}$ in MeOH-d_4 at 10 °C, 20 °C, 30 °C, 40 °C and 50 °C. The data was determined relative to the 20°C data from Table 3.

$[Eu.DOTA(MeOH\text{-}d_4)]^-$					
Temperature	Φ^a	k_r (s^{-1})	k_{nr} (s^{-1})	τ_{obs} (ms)	A_{MD} (s^{-1})
10°C	0.46	189	219	2.45	19.85
20°C	0.47	192	218	2.44	20.45
30°C	0.51	214	208	2.37	22.39
40°C	0.56	256	200	2.19	27.34
50°C	0.61	323	206	1.89	34.02
$[Eu(MeOH\text{-}\ d_4)_9]^{3+}$					
Temperature	Φ^a	k_r (s^{-1})	k_{nr} (s^{-1})	τ_{obs} (ms)	A_{MD} (s^{-1})
10°C	0.36	121	214	2.99	17.95
20°C	0.37	126	210	2.98	18.45
30°C	0.38	129	209	2.96	18.65
40°C	0.38	131	211	2.92	18.77
50°C	0.38	134	217	2.85	18.85

[a] See Table 3.

Conclusion

As data had suggested that there were fundamental questions in Eu^{3+} photophysics that remained unanswered, we set out to investigate the photophysical properties of $[Eu(MeOH\text{-}d_4)_9]^{3+}$ and $[Eu.DOTA(MeOH\text{-}d_4)]^-$ in MeOH-d_4 as a function of temperature in great detail.

We found that the light absorption by the intraconfigurational *f-f* transitions of the Eu^{3+} ions decreases as the temperature increases. This was rationalized by an increase in the symmetry of the average structure of the complexes in solution at higher temperatures.

We observed a significant self-quenching effect in these systems. We estimate the effect to be negligible at concentrations below 10mM in protonated solvents and below 4mM in deuterated solvents.

We saw that the excited state lifetime decreases when temperatures increase. This observation was challenged, and we found that it was exclusively due to an increase in the radiative rate constant. The increase in the rate of luminescence was much more pronounced for $[Eu.DOTA(MeOH\text{-}d_4)]^-$ than for $[Eu(MeOH\text{-}d_4)_9]^{3+}$. We can conclude that the relative transition probability of emission, A_{rel}, increases with increasing temperature in these systems. And we propose that this is because the higher thermal energy allows the complexes to visit more distorted structures during the excited state lifetime. These distorted structures will have a lower symmetry and thus a higher

probability of emission. The effect of these high emission probability conformations is an overall increase of the observed transition probability.

By determining the quantum yield of luminescence, the radiative and non-radiative rate constants were calculated. For $[Eu.DOTA(MeOH\text{-}d_4)]^-$, we conclude that k_r increases as temperature increases, while k_{nr} remains constant. We arrive at the same conclusion for $[Eu(MeOH\text{-}d_4)_9]^{3+}$ although change in k_r is less pronounced.

Finally, the data allowed us to conclude that the $^5D_0 \rightarrow {}^7F_1$ band is not independent of the surrounding environment as has previously been proposed by Werts.[6] And as A_{MD} values of 20.46 s^{-1} and 18.45 s^{-1} were determined here,[48] we urge great caution when one considers A_{MD} =14.65 s^{-1} constant across all Eu^{3+} complexes.

Thus we show that there are still unexplored aspects of Eu^{3+} photophysics, and we conclude that we need a new theoretical framework to rationalize the experimental observations.

AUTHOR INFORMATION

Corresponding Authors

*E-mail: TJS@chem.ku.dk.

ORCID

Nicolaj Kofod: 0000-0003-2905-8938

Lea Gundorff Nielsen: 0000-0001-7879-6115

Thomas Just Sørensen: 0000-0003-1491-5116

Notes

There are no competing financial interests to declare.

Supporting information

Supporting Information Available:

All optical spectra: absorption, luminescence emission, time-resolved emission decays and photophysical parameters as well as synthetic procedure.

Acknowledgements

The authors thank Carlsbergfondet, Villum Fonden (grant#14922), the University of Copenhagen, the Danish Chemical Society, and Fulbright Denmark for support. The authors also thank Niels Andreas Bonde, University of Copenhagen for his helpful discussions in preparing this manuscript.

References

1. Horrocks, W. D.; Sudnick, D. R., Lanthanide ion probes of structure in biology. Laser-induced luminescence decay constants provide a direct measure of the number of metal-coordinated water molecules. *Journal of the American Chemical Society* **1979,** *101* (2), 334-340.
2. Beeby, A.; Clarkson, I. M.; Dickins, R. S.; Faulkner, S.; Parker, D.; Royle, L.; de Sousa, A. S.; Williams, J. A. G.; Woods, M., Non-radiative deactivation of the excited states of europium, terbium and ytterbium complexes by proximate energy-matched OH, NH and CH oscillators: an improved luminescence method for establishing solution hydration states. *Journal of the Chemical Society, Perkin Transactions 2* **1999,** (3), 493-504.
3. Latva, M.; Takalo, H.; Mukkala, V. M.; Matachescu, C.; RodriguezUbis, J. C.; Kankare, J., Correlation between the lowest triplet state energy level of the ligand and lanthanide(III) luminescence quantum yield. *J. Luminescence* **1997,** *75* (2), 149-169.
4. Hehlen, M. P.; Brik, M. G.; Krämer, K. W., 50th anniversary of the Judd–Ofelt theory: An experimentalist's view of the formalism and its application. *Journal of Luminescence* **2013,** *136*, 221-239.
5. Karraker, D. G., Hypersensitive transitions of six-, seven-, and eight-coordinate neodymium, holmium, and erbium chelates. *Inorganic chemistry* **1967,** *6* (10), 1863-1868.
6. Werts, M. H. V.; Jukes, R. T. F.; Verhoeven, J. W., The emission spectrum and the radiative lifetime of Eu3+ in luminescent lanthanide complexes. *Physical Chemistry Chemical Physics* **2002,** *4* (9), 1542-1548.
7. Carnall, W. T.; Goodman, G. L.; Rajnak, K.; Rana, R. S., A systematic analysis of the spectra of the lanthanides doped into single crystal LaF3 *The Journal of chemical physics* **1989,** *90* (7), 3443-3457.
8. Carnall, W. T.; Crosswhite, H.; Crosswhite, H. M. *Energy level structure and transition probabilities in the spectra of the trivalent lanthanides in LaF₃*; ANL-78-XX-95; TRN: 79-005910 United States 10.2172/6417825 TRN: 79-005910 Dep. NTIS, PC A09/MF A01. ANL English; ; Argonne National Lab. (ANL), Argonne, IL (United States): 1978; p Medium: ED; Size: 195 p.
9. Binnemans, K., Interpretation of europium(III) spectra. *Coordination Chemistry Reviews* **2015,** *295*, 1-45.
10. Bünzli, J.-C. G.; Eliseeva, S. V., *Lanthanide Luminescence*. 2011.
11. Tanner, P. A., Some misconceptions concerning the electronic spectra of tri-positive europium and cerium. *Chemical Society Reviews* **2013,** *42* (12), 5090-5101.
12. Werts, M. H. V., Making sense of Lanthanide Luminescence. **2005,** *88* (2), 101-131.
13. Vereb, G.; Jares-Erijman, E.; Selvin, P. R.; Jovin, T. M., Temporally and Spectrally Resolved Imaging Microscopy of Lanthanide Chelates. *Biophys J* **1998,** *74* (5), 2210-2222.
14. Hemmilä, I.; Dakubu, S.; Mukkala, V.-M.; Siitari, H.; Lövgren, T., Europium as a label in time-resolved immunofluorometric assays. *Analytical Biochemistry* **1984,** *137* (2), 335-343.
15. Montgomery, C. P.; Murray, B. S.; New, E. J.; Pal, R.; Parker, D., Cell-Penetrating Metal Complex Optical Probes: Targeted and Responsive Systems Based on Lanthanide Luminescence. *Acc. Chem. Res.* **2009,** *42* (7), 925-937.
16. Kofod, N.; Nawrocki, P.; Juelsholt, M.; Christiansen, T. L.; Jensen, K. M. Ø.; Sørensen, T. J., Solution Structure, Electronic Energy Levels, and Photophysical Properties of [Eu(MeOH)n−2m(NO3)m]3−m+ Complexes. *Inorganic Chemistry* **2020**.
17. Caravan, P.; Ellison, J. J.; McMurry, T. J.; Lauffer, R. B., Gadolinium(III) chelates as MRI contrast agents: Structure, dynamics, and applications. *Chemical Reviews* **1999,** *99* (9), 2293-2352.
18. Sørensen, T. J.; Faulkner, S., Multimetallic Lanthanide Complexes: Using Kinetic Control To Define Complex Multimetallic Arrays. *Acc Chem Res* **2018,** *51* (10), 2493-2501.
19. Nielsen, L. G.; Junker, A. K. R.; Sørensen, T. J., Composed in the f-block: solution structure and function of kinetically inert lanthanide(iii) complexes. *Dalton transactions* **2018,** *47* (31), 10360-10376.
20. Drew, M. G., Structures of high coordination complexes. *Coordination Chemistry Reviews* **1977,** *24* (2-3), 179-275.
21. Llunell, M. J. C. E. J., SHAPE, v1. 1b, University of Barcelona, 2005 Search PubMed;(b) A. Ruiz-Martínez, D. Casanova and S. Alvarez. **2008,** *14*, 1291-1303.
22. Nielsen, L. G.; Sørensen, T. J., Including and Declaring Structural Fluctuations in the Study of Lanthanide(III) Coordination Chemistry in Solution. *Inorganic chemistry* **2019,** *59* (1), 94-105.
23. Helm, L.; Merbach, A. E., Inorganic and bioinorganic solvent exchange mechanisms. *Chem Rev* **2005,** *105* (6), 1923-59.
24. Nawrocki, P. R.; Kofod, N.; Juelsholt, M.; Jensen, K. M. Ø.; Sørensen, T. J., The effect of weighted averages when determining the speciation and structure–property relationships of europium(iii) dipicolinate complexes. *Physical Chemistry Chemical Physics* **2020,** *22* (22), 12794-12805.
25. Tanner, P. A.; Zhou, L.; Duan, C.; Wong, K.-L., Misconceptions in electronic energy transfer: bridging the gap between

chemistry and physics. *Chemical Society reviews* **2018,** *47* (14), 5234-5265.

26. Strickler, S. J.; Berg, R. A., Relationship between absorption intensity and fluorescence lifetime of molecules. *J. Chem. Phys.* **1962,** *37* (4), 814-&.

27. Hirayama, S.; Phillips, D., Correction for refractive index in the comparison of radiative lifetimes in vapour and solution phases. *J. Photochem.* **1980,** *12* (2), 139-145.

28. Turro, N. J., *Modern Molecular Photochemistry* University Science Books Sausalito, 1991; p 628.

29. Kofod, N.; Arppe-Tabbara, R.; Sørensen, T. J., Electronic Energy Levels of Dysprosium(III) ions in Solution. Assigning the Emitting State and the Intraconfigurational 4f–4f Transitions in the Vis–NIR Region and Photophysical Characterization of Dy(III) in Water, Methanol, and Dimethyl Sulfoxide. *The Journal of Physical Chemistry A* **2019,** *123* (13), 2734-2744.

30. Kasha, M., From Jablonski to femtoseconds. Evolution of molecular photophysics. *Acta Phys. Pol. A* **1999**, 15-36.

31. Dai, H.; Stafsudd, O. M., Polarized absorption spectrum and intensity analysis of trivalent neodymium in sodium β″ alumina. *Journal of Physics and Chemistry of Solids* **1991,** *52* (2), 367-379.

32. Desreux, J. F. J. I. c., Nuclear magnetic resonance spectroscopy of lanthanide complexes with a tetraacetic tetraaza macrocycle. Unusual conformation properties. **1980,** *19* (5), 1319-1324.

33. Junker, A. K. R.; Tropiano, M.; Faulkner, S.; Sørensen, T. J. J. I. c., Kinetically inert lanthanide complexes as reporter groups for binding of potassium by 18-crown-6. **2016,** *55* (23), 12299-12308.

34. Würth, C.; Grabolle, M.; Pauli, J.; Spieles, M.; Resch-Genger, U., Relative and absolute determination of fluorescence quantum yields of transparent samples. *Nature Protocols* **2013,** *8* (8), 1535-1550.

35. Resch-Genger, U.; Hoffmann, K.; Nietfeld, W.; Engel, A.; Neukammer, J.; Nitschke, R.; Ebert, B.; Macdonald, R., How to Improve Quality Assurance in Fluorometry: Fluorescence-Inherent Sources of Error and Suited Fluorescence Standards. *Journal of Fluorescence* **2005,** *15* (3), 337-362.

36. Demas, J. N.; Crosby, G. A., The Measurement of Photoluminescence Quantum Yields. A Review. *Journal of Physical Chemistry* **1971,** *75*.

37. Groot, M.-L.; Peterman, E.; van Kan, P.; van Stokkum, I.; Dekker, J. P.; van Grondelle, R. J. B. j., Temperature-dependent triplet and fluorescence quantum yields of the photosystem II reaction center described in a thermodynamic model. **1994,** *67* (1), 318-330.

38. Esteban-Gómez, D.; Büldt, L. A.; Pérez-Lourido, P.; Valencia, L.; Seitz, M.; Platas-Iglesias, C., Understanding the Optical and Magnetic Properties of Ytterbium(III) Complexes. *Inorganic Chemistry* **2019,** *58* (6), 3732-3743.

39. Duan, C.-K.; Tanner, P. A., What Use Are Crystal Field Parameters? A Chemist's Viewpoint. *The Journal of Physical Chemistry A* **2010,** *114* (19), 6055-6062.

40. Bowen, E. J.; Sahu, J., The Effect of Temperature on Fluorescence of Solutions. *The Journal of Physical Chemistry* **1959,** *63* (1), 4-7.

41. Richardson, F. S., Selection rules for lanthanide optical activity. *Inorganic chemistry* **1980,** *19* (9), 2806-2812.

42. Riehl, J. P.; Richardson, F. S., CIRCULARLY POLARIZED LUMINESCENCE SPECTROSCOPY. *Chem. Rev.* **1986,** *86* (1), 1-16.

43. Kavarnos, G. J., *Fundamentals of photoinduced electron transfer*. VCH New York etc: 1993; Vol. 1.

44. Karraker, D. G. J. I. C., Hypersensitive transitions of six-, seven-, and eight-coordinate neodymium, holmium, and erbium chelates. **1967,** *6* (10), 1863-1868.

45. Charbonniere, L. J.; Hildebrandt, N.; Ziessel, R. F.; Lohmannsroben, H. G., Lanthanides to quantum dots resonance energy transfer in time-resolved fluoro-immunoassays and luminescence microscopy. *Journal of the American Chemical Society* **2006,** *128* (39), 12800-9.

46. Chen, C.; Ao, L.; Wu, Y. T.; Cifliku, V.; Cardoso Dos Santos, M.; Bourrier, E.; Delbianco, M.; Parker, D.; Zwier, J. M.; Huang, L.; Hildebrandt, N., Single-Nanoparticle Cell Barcoding by Tunable FRET from Lanthanides to Quantum Dots. *Angewandte Chemie* **2018,** *57* (41), 13686-13690.

47. Ware, W. R. J. T. J. o. P. C., Oxygen quenching of fluorescence in solution: an experimental study of the diffusion process. **1962,** *66* (3), 455-458.

48. Aebischer, A.; Gumy, F.; Bunzli, J. C., Intrinsic quantum yields and radiative lifetimes of lanthanide tris(dipicolinates). *Physical chemistry chemical physics : PCCP* **2009,** *11* (9), 1346-53.